Enhancement of Sono-Fenton by P25-Mediated Visible Light Photocatalysis: Analysis of Synergistic Effect and Influence of Emerging Contaminant Properties

Lanyue Qi [1], Wenyuan Lu [1], Gengxu Tian [1], Yang Sun [1], Jiangang Han [1,2,3,*] and Lijie Xu [1,*]

[1] College of Biology and the Environment, Nanjing Forestry University, Nanjing 210037, Jiangsu, China; qilanyue@163.com (L.Q.); wennerlu@163.com (W.L.); GengXu_Tian@163.com (G.T.); sunyang@njfu.edu.cn (Y.S.)

[2] Co-Innovation Center for the Sustainable Forestry in Southern China, Nanjing Forestry University, Nanjing 210037, Jiangsu, China

[3] National Positioning Observation Station of Hung-tse Lake Wetland Ecosystem, Hongze 223100, Jiangsu, China

* Correspondence: hjg@njfu.edu.cn (J.H.); xulijie@njfu.edu.cn (L.X.); Tel.: +86-025-85427312 (J.H.); +86-156-51721667 (L.X.)

Abstract: The main purpose is to figure out the involved synergistic effects by combining sono-Fenton using in situ generated H_2O_2 and the photocatalytic process of P25 under visible light (Vis/P25). Two emerging contaminants, dimethyl phthalate (DMP) and diethyl phthalate (DEP), with similar structure but different properties were selected to examine the influence of hydrophilic and hydrophobic properties of target pollutants. Results show that there is synergy between sono-Fenton and Vis/P25, and more significant synergy can be obtained with low dose of Fe^{3+} or Fe^{2+} (0.02 mM) and for more hydrophilic DMP. Based on systematic analysis, the primary mechanism of the synergy is found to be the fast regeneration of Fe^{2+} by photo-electrons from P25 photocatalysis, which plays the dominant role when the Fe^{3+}/Fe^{2+} concentration is low (0.02 mM). However, at high Fe^{3+}/Fe^{2+} concentration (0.5 mM), the photoreduction of Fe(III) to Fe^{2+} can play a key role with relatively low efficiency. By studying the degradation intermediates of both DMP and DEP, the degradation pathways can be determined as the hydroxylation of aromatic ring and the oxidation of the aliphatic chain. Better mineralization performance is achieved for DMP than that for DEP due to the enhanced utilization efficiency of H_2O_2 by accelerating Fe^{2+} regeneration.

Keywords: sono-Fenton; photocatalysis; TiO_2; P25; ultrasound; visible light; iron; cycling; emerging contaminant; endocrine disrupting compound

1. Introduction

The shortage of water resources accelerates the process of wastewater recycling, in which process the safety of reclaimed water should be the primary concern. The emerging contaminants (ECs), mainly consisting of the endocrine disrupting compounds (EDCs) and pharmaceuticals and personal care products (PPCPs), have the characteristics of chemical structure stability and resistance to biodegradation [1–3]. Although conventional wastewater treatment technologies present the opportunity for ECs removal, satisfactory removal techniques are still to be established.

The advanced oxidation technologies (AOTs) have shown excellent performance in degrading refractory organic pollutants by various radicals [4–9], although several technical challenges still have

to be addressed in future research before practical application. Due to the limitation of a single type of AOT, combinative technologies are often adopted to overcome the limitation and/or obtain synergistic performance. Among various AOTs, the ultrasound-based technologies have drawn increasing attention in different fields of wastewater treatment, such as assisting persulfate degradation of organic contaminants [10], treating the secondary effluent of a municipal wastewater before agricultural reuse [11], serving the pretreatment of edible oil wastewater before the biological treatment [12,13], and destroying wastewater particles for improved UV disinfection [14]. The typical characteristics of ultrasonic reactions are reflected by the heterogeneous distribution of solutes including both pollutants and other water quality components due to the presence of cavitation gas bubbles, and also the in situ generated H_2O_2 with zero-order kinetics as mainly produced by the unutilized hydroxyl radicals $(2\bullet OH \rightarrow H_2O_2)$ [15–17]. Other AOTs are often tried to combine with ultrasound (US) to make full use of the in situ generated H_2O_2, like the combinative technologies of UV/US [18,19], sono-Fenton process [20,21], and US/O_3 [22].

The combination of US and homogeneous Fenton to create sono-Fenton process is a simple and environmentally friendly approach. In sono-Fenton process, the increase of Fe^{2+} concentration can to some extent enhance the efficiency of pollutants degradation [23]. However, since Fe^{2+} itself also consumes the reactive oxygen species (ROS), simply increasing Fe^{2+} concentration not only results in unproductive consumption of H_2O_2 in the system but also easily produces iron sludge waste. In conventional Fenton system, Fe^{2+} plays the role of a reactant rather than a catalyst since its consumption rate is very fast and the regeneration rate is rather slow. Promoting Fe^{2+} regeneration in Fenton-related processes can not only fully cut down the iron demand but also improve the utilization efficiency of H_2O_2, changing the role of Fe^{2+} more like a catalyst.

The photo-electrons generated from various kinds of photocatalysts can effectively reduce ferric ions to ferrous ions [24,25]. The previous study of this (Xu et al., 2019) finds that, through the interactions between P25 and Fenton reagent, the photoelectrons can be more efficiently excited by visible light, which further significantly accelerates Fe^{3+} reduction and promotes iron cycling in photo-Fenton process. As a result, the iron demand is decreased and the use of H_2O_2 is more productive [26]. Inspired from these findings, the P25-mediated visible light condition was tried to combine with sono-Fenton to examine the possibility of improving the efficiency with exclusive in situ produced H_2O_2 [23]. It is found that the presence of P25 accelerates the degradation of sulfadiazine at small amount of iron precursors (Fe^{2+}/Fe^{3+}) (0.02 mM) and free of exogenous H_2O_2, making the regeneration of Fe^{2+} much faster than that in sono-Fenton process [23]. However, the synergistic effects and detailed mechanisms of combining sono-Fenton and the photocatalytic process of P25 have not yet been systematically investigated. Additionally, the relationship between the process synergy and pollutant properties has not been investigated previously.

Two EDCs, dimethyl phthalate (DMP) and diethyl phthalate (DEP), belonging to the group of phthalate acid esters (PAEs), are selected as the target pollutants. The PAEs are mainly used as plasticizers to improve the ductility and softness of various products [27]. Both DMP and DEP are classified as the "priority-controlled toxic pollutants" by the US Environmental Protection Agency. The similar chemical structures but different side chain lengths for DMP and DEP can make them demonstrate different physicochemical properties.

In view of the above, the main purpose of this study is to figure out the involved mechanisms and the synergistic effects by combining sono-Fenton using in situ generated H_2O_2 and the photocatalytic process of P25 under visible light (Vis/P25) when degrading refractory organic pollutants. The influence of physicochemical properties of target pollutants is also to be discussed.

2. Results and Discussion

2.1. Synergy Between Sono-Fenton and Vis/P25

The degradation kinetics of DEP and DMP in the processes of P25 photocatalysis (Vis/P25), sono-Fenton (US/Fe^{2+}), and the coupling (Vis/P25 + US/Fe^{2+}) is shown in Figure 1. The pseudo first-order rate constants and corresponding R^2 values of the fitting for different processes are summarized in Table 1. A very low amount of Fe^{2+} (0.02 mM) was applied to examine the synergistic effects. In Vis/P25 process (Figure 1), a small amount of adsorption occurs in dark for both compounds, but their degradation is insignificant under visible light irradiation. The pseudo first-order rate constants of DEP and DMP photocatalysis are only 0.0009 min^{-1} and 0.0003 min^{-1}, respectively. This is on the one hand due to the very limited overlap between the absorption edge of P25 (*ca.* 420 nm) and the emission spectrum of the light emitting diode (LED) lamp (Figure S1). On the other hand, the superoxide radicals (O$_2{}^{\bullet-}$) have been reported as the important reactive oxygen species (ROS) in the photocatalytic process of P25 [28,29], which however are incapable to decompose the structures like DMP [30,31]. In sono-Fenton process, both DEP and DMP can be degraded efficiently with the rate constants of 0.0400 min^{-1} and 0.0287 min^{-1}, respectively (Table 1, line 3). However, it is noticed that the sono-Fenton process doped with 0.02 mM Fe^{2+} only makes limited improvement compared with the sole ultrasonic process (line 1), probably due to the fast consumption of 0.02 mM Fe^{2+}. However, the degradation of both compounds is accelerated significantly in the coupling processes of Vis/P25 + US/Fe^{2+} (Figure 1). The synergy indexes (SI) as determined from Equation (1) are 2.65 and 2.41 for DMP and DEP, respectively, based on the pseudo first-order rate constants shown in Table 1. The SI > 1 indicates the existing synergy between two processes and stronger synergy is obtained for the degradation of DMP. The involved mechanisms will be discussed in more detail below.

$$\text{Synergy Index} = \frac{k_{(\text{Vis/P25 }+\text{US/Fe2+})}}{k_{(\text{Vis/P25}) }+k_{(\text{US/Fe2+})}} \tag{1}$$
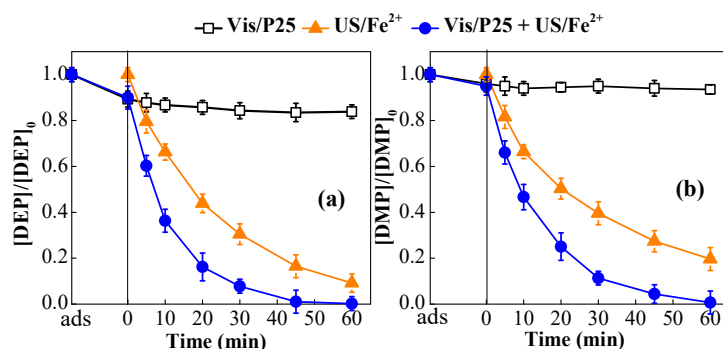

Figure 1. The degradation kinetics of diethyl phthalate (DEP) (**a**) and dimethyl phthalate (DMP) (**b**) in the processes of P25 photocatalysis (Vis/P25), sono-Fenton (US/Fe^{2+}), and the coupling (Vis/P25 + US/Fe^{2+}) (conditions: [DMP]$_0$ = 0.01 mM, [DEP]$_0$ = 0.01 mM, P25 dosage 0.5 g L^{-1}, adsorption time 20 min, [Fe^{2+}]$_0$ = 0.02 mM).

Table 1. The pseudo first-order degradation rate constants of both DMP and DEP in US and sono-Fenton processes with two different iron levels (0.02 mM and 0.5 mM).

	Processes	DMP			DEP		
		$k_{average}$ (min^{-1})	R^2	SI	$k_{average}$ (min^{-1})	R^2	SI
1	US	0.0252	0.9774		0.0375	0.9927	
2	Vis/P25	0.0003	0.9494		0.0009	0.9345	
3	Sono-Fenton	US/Fe^{2+} (0.02 mM)	0.9784		0.0400	0.9996	
4		US/Fe^{3+} (0.02 mM)	0.9921		0.0383	0.9986	
5		US/Fe^{2+} (0.5 mM)	0.9874		0.0619	0.9917	
6		US/Fe^{3+} (0.5 mM)	0.9983		0.0418	0.9964	
7	Visible light assisted sono-Fenton	US/Fe^{2+} + Vis (0.02 mM)	0.9792		0.0494	0.9950	
8		US/Fe^{3+} + Vis (0.02 mM)	0.9921		0.0403	0.9998	
9		US/Fe^{2+} + Vis (0.5 mM)	0.9778		0.0722	0.9661	
10		US/Fe^{3+} + Vis (0.5 mM)	0.9990		0.0548	0.9940	
11	P25 mediated sono-Fenton	US/Fe^{2+} + Vis/P25 (0.02 mM)	0.9843	2.65	0.0987	0.9918	2.41
12		US/Fe^{3+} + Vis/P25 (0.02 mM)	0.9812	2.91	0.1051	0.9904	2.68
13		US/Fe^{2+} + Vis/P25 (0.5 mM)	0.9863	1.64	0.0848	0.9879	1.35
14		US/Fe^{3+} + Vis/P25 (0.5 mM)	0.9804	1.86	0.0730	0.9932	1.71

Note: rows 3–14 $k_{average}$ DMP values: 3: 0.0287, 4: 0.0276, 5: 0.0424, 6: 0.0326, 7: 0.0289, 8: 0.0297, 9: 0.0443, 10: 0.0398, 11: 0.0768, 12: 0.0812, 13: 0.0700, 14: 0.0612

2.2. Influence of P25 on Ultrasonic and Sono-Fenton Processes in Dark

In order to clarify the involved synergistic mechanisms of combining sono-Fenton and the photocatalytic process of P25, influence of P25 on both ultrasonic and sono-Fenton processes was firstly examined in dark. Varied dosages of P25 (0~0.8 g/L) were added in ultrasonic processes to examine the impact. As observed in Figure S2, the presence of P25 slightly enhances the removal of both pollutants as the increase of dosages from 0 to 0.5 g·L^{-1}. This may be resulting from the increased nuclei for cavitation bubble formation by fine particles of P25 [32]. However, further increase of the dosages to 0.8 g·L^{-1} makes slight deceleration of pollutants removal, which may be related with the attenuation of ultrasound intensity by the presence of excess particles. In addition, a large amount of P25 may also shield incident light, so 0.5 g·L^{-1} P25 as observed as the optimum dosage in Figure S2 was selected for further tests. The ultrasonic degradation kinetics of both DMP and DEP with and without the presence of P25 is shown in Figure S3. During the 20 min silent adsorption (stirring in beaker without ultrasound input), a higher ratio of adsorption is obtained for DEP (12%) compared to that for DMP (5%), which can be attributed to the stronger hydrophobicity of DEP (logKow = 2.47) than that of DMP (logKow = 1.60). During the ultrasonic reaction, DEP removal in the presence of P25 demonstrates gradual convergence with that of the ultrasonic process since the adsorbed DEP molecules can get redissolved under the shock of ultrasonic waves. In general, the influence of P25 on ultrasonic degradation of both DMP and DEP is weak.

Further, the influence of P25 on dark sono-Fenton was examined with results shown in Figure 2. Since Fe^{2+} and Fe^{3+} are interconvertible in the presence of light, both were tried as precursors in sono-Fenton reaction. Figure 2 shows that Fe^{2+} ions are more efficient to initiate the sono-Fenton reaction compared with Fe^{3+}, leading to faster degradation of both DMP and DEP in US/Fe^{2+} processes. It is found that the presence of P25 does not hinder compounds degradation. Although the possible adsorption of Fe^{2+} and Fe^{3+} on P25 may reduce the amount of iron to react with H_2O_2, further stripping by ultrasonic shock and the additional nuclei provided by P25 for ultrasonic cavitation may slightly promote the degradation of DMP and DEP instead. The 60 min removal rates in the above-mentioned processes are compared in Figure S4, where positive effects of P25 addition can be clearly seen on both ultrasonic and dark sono-Fenton processes. This provides favorable conditions for the combination of sono-Fenton and P25-mediated photocatalysis. In general, in the absence of visible light, the influence of P25 is generally weak and other mechanisms should be involved.
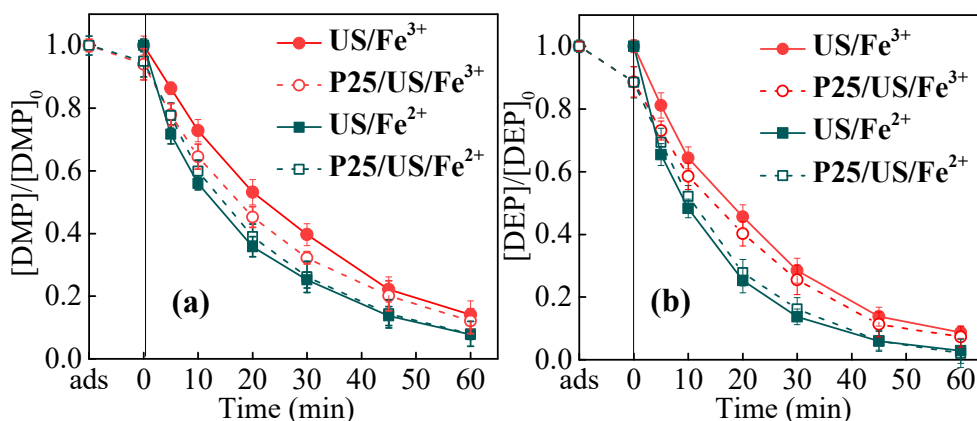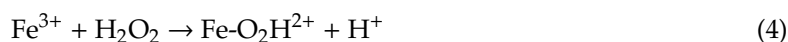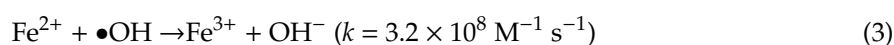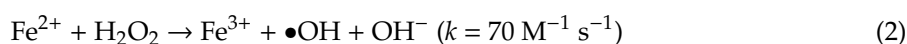
Figure 2. Influence of P25 on the degradation of (**a**) DMP and (**b**) DEP in dark sono-Fenton and sono-Fenton-like processes ($[DMP]_0 = 0.01$ mM, $[DEP]_0 = 0.01$ mM, P25 dosage 0.5 g L^{-1}, adsorption time 20 min, $[Fe^{2+}]_0 = 0.5$ mM, $[Fe^{3+}]_0 = 0.5$ mM).

2.3. Transformation of Iron in Dark Sono-Fenton

In sono-Fenton process, the role of iron species can be double-edged. Increase of Fe^{2+} concentration can promote Fenton reaction (Equation (2)), but the self-quenching property of Fe^{2+} is also able to slow down the degradation of pollutants (Equation (3)) [23,33]. As shown in Table 1, when increasing the initial iron concentrations from 0.02 mM to 0.5 mM (lines 3–6), the pollutant removal efficiency increases significantly. By examining the variation trends of ferrous irons (Figure 3), it is found that in dark sono-Fenton processes, the Fe^{2+} concentration decreased dramatically due to the fast reaction between Fe^{2+} and H_2O_2. Especially when the initial concentration of Fe^{2+} is low at 0.02 mM (Figure 3b), the vast majority is consumed within 10 min, which explains well the limited improvement of pollutant degradation in this condition compared with US alone (Table 1). Thus, the available Fe^{2+} in dark sono-Fenton process mainly lies on its initial dose. Although the ultrasonic wave has been reported to facilitate Fe^{3+} reduction (Equations (4) and (5)) [34,35] and compounds degradation is also improved when applying high Fe^{3+} dose (0.5 mM) as shown in Table 1 (line 6), the available Fe^{2+} measured in dark US/Fe^{3+} process is at low level (Figure 3). This may be because the sono-reduction of Fe^{3+} is a rate-limiting step and Fe^{2+} can immediately react with H_2O_2 once produced without obvious accumulation. It is also observed that, the sono-Fenton processes doped with 0.02 mM Fe^{2+} or Fe^{3+} shows similar efficiencies in degrading compounds (lines 3, 4 in Table 1), which agrees with the close level of detectable Fe^{2+} concentration in US + Fe^{2+} and US + Fe^{3+} processes after 10 min reaction (Figure 3b). On the contrary, with 0.5 mM of iron, the US + Fe^{2+} process shows much higher efficiency than US + Fe^{3+} (lines 9, 10), which is owing to the higher amount of Fe^{2+} in US + Fe^{2+} process throughout the 60 min reaction as shown in Figure 3a. Moreover, it is also found that, when the Fe^{2+} is at low level (0.02 mM) (Figure 3b), the consumption of Fe^{2+} during the degradation of DMP (dotted line) proceeds more quickly than that in the process of DEP degradation (solid line). This is because DMP is relatively hydrophilic and its direct ultrasonic oxidation is not so efficient as that of DEP, resulting in higher level of underutilized H_2O_2 and the eventual stronger ability to consume Fe^{2+}. As a result, the degradation of DMP is enhanced more obviously than that of DEP in dark sono-Fenton processes.
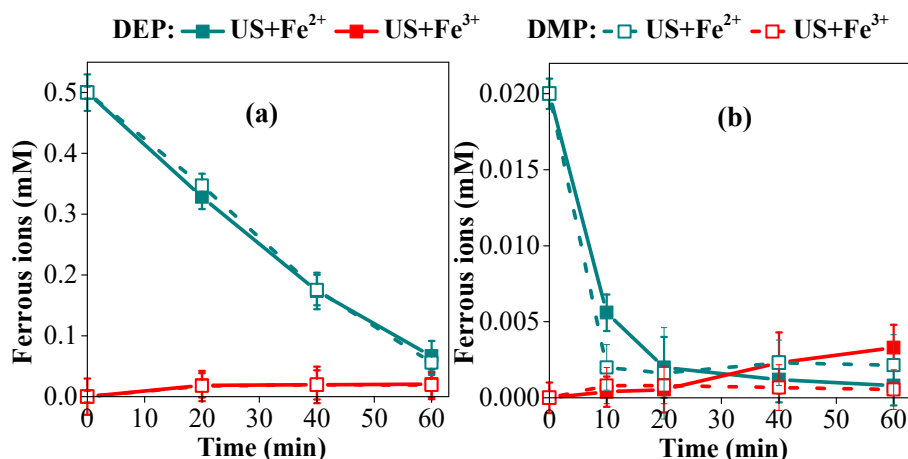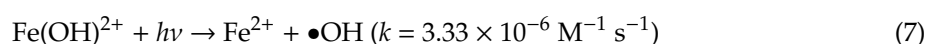
$$Fe^{2+} + H_2O_2 \rightarrow Fe^{3+} + \bullet OH + OH^- \ (k = 70 \ M^{-1} \ s^{-1}) \tag{2}$$

$$Fe^{2+} + \bullet OH \rightarrow Fe^{3+} + OH^- \ (k = 3.2 \times 10^8 \ M^{-1} \ s^{-1}) \tag{3}$$

$$Fe^{3+} + H_2O_2 \rightarrow Fe\text{-}O_2H^{2+} + H^+ \tag{4}$$

$$Fe\text{--}O_2H^{2+} +))) \rightarrow Fe^{2+} + \bullet OOH \tag{5}$$

Figure 3. Variation of ferrous ion concentrations during the degradation of DMP or DEP in sono-Fenton and sono-Fenton-like processes at two different levels of iron species: (**a**) 0.5 mM, (**b**) 0.02 mM ([DMP]$_0$ = 0.01 mM, [DEP]$_0$ = 0.01 mM).

2.4. Influence of Visible Light on Sono-Fenton Processes

Based on the above investigation, the main problems of dark sono-Fenton and sono-Fenton like processes are the strong dependence on the large initial dose of iron and the slow regeneration of Fe^{2+}. Herein, the influence of visible light on sono-Fenton processes was examined mainly focusing on the interactions between visible light and iron.

The influence of visible light was first examined by evaluating the compounds degradation. As can be seen in Table 1, in the presence of visible light (lines 7, 8), compounds degradation at 0.02 mM Fe^{2+}/Fe^{3+} concentrations shows similar rates with that in sono-Fenton processes (lines 3, 4), suggesting the weak interactions between iron species and visible light. In general, the light absorption of both Fe^{2+} and Fe^{3+} in visible range is weak (Figure S5), particularly at low concentrations. Therefore, the direct photo-transformation of iron should be weak at 0.02 mM. When increasing the Fe^{2+}/Fe^{3+} concentrations to 0.5 mM, moderate enhancement of compounds degradation induced by visible light is observed (lines 5, 6 and lines 9, 10), which is more remarkable for DEP degradation. The pseudo first-order rate constants of DEP decomposition increased by 17% and 31% due to the presence of visible light for using Fe^{2+} or Fe^{3+} (0.5 mM) as the precursor, respectively. Influence of Fe^{2+}/Fe^{3+} photoactivities on compounds degradation is separately investigated by control experiments conducted in Vis+Fe^{2+}/Fe^{3+} process without ultrasound (Figure S6). It is clearly seen that, photolysis of Fe(III) could lead to compounds degradation mainly due to the generation of •OH radicals (Equations (6) and (7)), and the efficiency is associated with Fe^{3+} concentration. Hardly any degradation is observed for both compounds during the photolysis of Fe^{2+}. It is also observed that DEP degradation proceeds slightly faster than DMP probably ascribed to their different reaction rates with •OH radicals ($k_{•OH,DMP} = 3.46 \times 10^8$ M^{-1} s^{-1}, $k_{•OH,DEP} = 2.09 \times 10^9$ M^{-1} s^{-1}) [36]. This may also explain the above-mentioned greater impact induced by visible light for DEP degradation in sono-Fenton process.

$$Fe^{3+} + H_2O \rightarrow Fe(OH)^{2+} + H^+ \tag{6}$$

$$Fe(OH)^{2+} + h\nu \rightarrow Fe^{2+} + •OH \quad (k = 3.33 \times 10^{-6} \text{ M}^{-1} \text{ s}^{-1}) \tag{7}$$

As observed in Figure S7, Fe^{2+} concentration in the presence of visible light shows similar variation trends as that in dark sono-Fenton (Figure 3). The moderate enhancement by visible light at 0.5 mM iron dosage (lines 5, 6 and lines 9, 10) indicates additional sources of radicals most likely by improved decomposition of H_2O_2, while the insignificant difference of Fe^{2+} variation as shown in Figure 3 and Figure S7 implies a possible fast circulation between Fe^{2+} and Fe^{3+}. As reported, the Fe(II) can be photo-oxidized to Fe(III) by UV light and even filtered light of λ > 400 nm [37,38] and Fe(III) is

also well known for its photoactivity (Equations (6) and (7)), leading to the promoted conversion of $Fe^{2+} \rightarrow Fe^{3+}$ and $Fe^{3+} \rightarrow Fe^{2+}$ under visible light. From the control experiment results, it is assumed that at relatively high concentration of iron dose (0.5 mM), photolysis of Fe(III) can play a role in compounds degradation, while it is negligible at low level of iron (0.02 mM).

2.5. Role of the Photoelectrons in Promoting Fe^{2+} Regeneration

The role of P25 in promoting Fe^{3+} reduction was firstly examined without ultrasound input to examine the Fe^{2+} generation capability (Figure 4). At 0.5 mM Fe^{3+} conditions (green lines), the production of Fe^{2+} in the presence of P25 shows similar rates as when you use light only, suggesting the role of direct light reduction of Fe^{3+} dominates (Equations (6) and (7)). However, at 0.02 mM Fe^{3+} conditions (red lines), the presence of P25 significantly promotes the generation of Fe^{2+}, roughly four times the amount of direct light reduction, implying that Fe^{3+} reduction by photoelectrons generated from P25 (Equations (8) and (9)) is more efficient than visible light reduction [26]. Due to the limitation of active sites on P25 surface and the mobility of Fe^{3+} ions, the superiority of photoelectrons in Fe^{3+} reduction is more remarkable at low iron concentrations. Moreover, it is also seen that in homogeneous conditions (free of cavitation bubbles) and in the absence of ultrasonically produced H_2O_2, the generation of Fe^{2+} is hardly influenced by the properties of target pollutants. This also implies that the discrepancies of process synergy obtained for DMP and DEP is primarily due to the heterogeneous effect during the occurrence of cavitation.
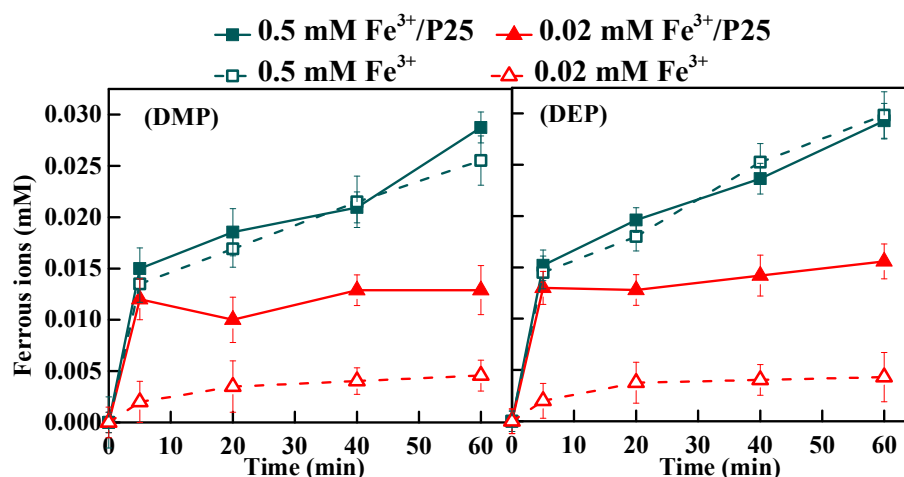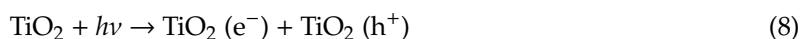
$$TiO_2 + h\nu \rightarrow TiO_2\ (e^-) + TiO_2\ (h^+) \tag{8}$$

$$TiO_2\ (e^-) + Fe^{3+} \rightarrow TiO_2 + Fe^{2+} \tag{9}$$

Figure 4. The reduction of ferric iron under visible light irradiation with and without the presence of P25 ([DMP]$_0$ = 0.01 mM, [DEP]$_0$ = 0.01 mM, P25 0.5 g L^{-1}).

Further, the variation of Fe^{2+} was examined in the presence of ultrasound (Figure 5). By comparing Figure S7a and Figure 5a (0.5 mM iron), the presence of P25 does not influence the detectable Fe^{2+} concentration in reaction system, but compounds degradation is improved moderately by comparing the kinetics data shown Table 1 (lines 9, 10 vs. lines 13, 14). From the analysis of Fe^{2+} in dark sono-Fenton (Figure 3a) and visible light assisted sono-Fenton (Figure S7a), it can be seen that when dosing 0.5 mM Fe^{2+} at the beginning, the remaining Fe^{2+} during the reaction is sufficient to conduct Fenton reaction, which is not the rate-limiting factor. Therefore, the improvement of compounds degradation at high level of Fe^{2+}/Fe^{3+} (0.5 mM) may not be ascribed to enhanced Fe^{2+} regeneration. Based on the investigation of photo-Fenton-like process, interactions are confirmed between P25 and Fe^{3+}, P25 and H_2O_2, respectively, which could enhance the generation of hydroxyl radicals mainly via

broadening the light absorption range of P25 and increasing the separation efficiency of photo-induced carriers [26]. This may also explain the enhanced compounds degradation in US/Fe^{2+} + Vis/P25 and US/Fe^{3+} + Vis/P25 processes with higher dosages (0.5 mM) of iron species.
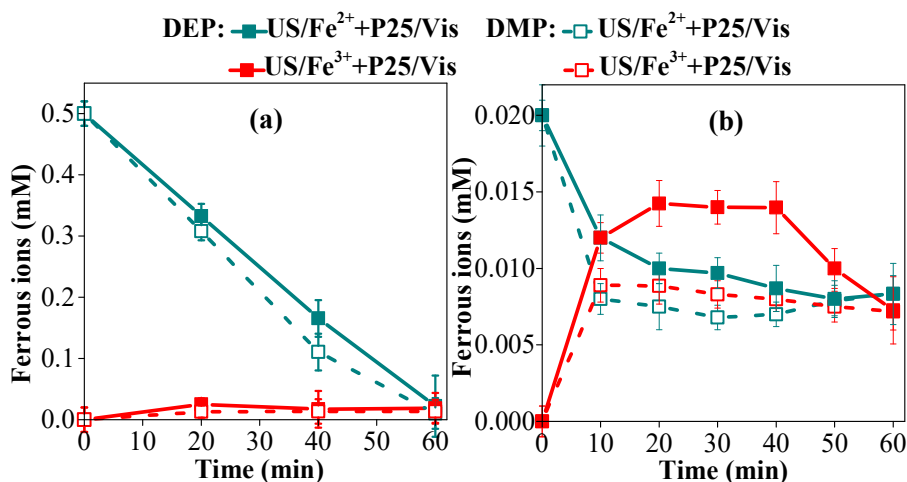

Figure 5. Variation of ferrous ion concentrations during the degradation of DMP or DEP in the combined processes of sono-Fenton and P25-mediated visible light photocatalysis at two different levels of iron species: (**a**) 0.5 mM, (**b**) 0.02 mM ([DMP]0 = 0.01 mM, [DEP]0 = 0.01 mM, P25 dosage 0.5 g L^{-1}).

However, it is clearly found from Figure 5b that, when doped with 0.02 mM Fe^{2+} (or Fe^{3+}), a relatively stable concentration of Fe^{2+} can be detected. It indicates that the Fe(III) reduction rate by photo-electrons is comparable to the Fe^{2+} oxidation rate in sono-Fenton process. Specifically, when using Fe^{2+} as the precursor (green lines), a fast decrease of [Fe^{2+}] can still be found within initial 10 min, while the steady-state concentrations of Fe^{2+} is significantly higher than that in dark sono-Fenton (Figure 3b). Moreover, faster generation and accumulation of Fe^{2+} is observed when using 0.02 mM Fe^{3+} as the precursor. By comparing the kinetic data shown in Table 1, the remarkable enhancement of compound degradation (lines 11, 12) from 0.0287 min^{-1} to 0.0768 min^{-1} and 0.0276 min^{-1} to 0.0812 min^{-1} when using Fe^{2+} and Fe^{3+} as the precursor, respectively, corresponds well with the increased regeneration of Fe^{2+} by photo-electrons. In addition, it is also illustrated in Figure 5b, the overall concentration of Fe^{2+} shows a higher level during the degradation of DEP than that of DMP, implying a relatively slow use of Fe^{2+} during the degradation of DEP due to its hydrophobic property. As a result, higher synergistic effects are obtained for the degradation of DMP (Table 1). In the late phase of the reaction, DEP has been mostly decomposed to more hydrophilic intermediates resulting in higher probabilities for the in situ accumulation of H$_2$O$_2$ and corresponding increased consumption of Fe^{2+}. Resultantly, the concentration of Fe^{2+} shows observable decrease after 40 min reaction.

Through the analysis, it can be confirmed that combining sono-Fenton process with P25-mediated photocatalysis under visible light can successfully realize the continuous supply of Fe^{2+} to react with H$_2$O$_2$ with low iron demand.

2.6. Analysis of the Intermediates and Mineralization Performance

The degradation pathways of both DMP and DEP were further investigated by identifying their degradation intermediates in US/Fe^{3+} + Vis/P25 (0.02 mM) process which demonstrates the highest synergistic effect. In order to intensify the mass signal of trace amount of intermediates and to facilitate the measurement of total organic carbon (TOC), 0.05 mM initial concentration was applied for both DMP and DEP. The high performance liquid chromatography (HPLC) spectra during the degradation of DMP and DEP were shown in Figure S8. It can be seen that the peak intensity of target compounds (i.e., DMP and DEP) gradually decreases as the reaction goes on, and complete disappear after 60 min. At the same time, some peaks assigned for various intermediates (e.g., 12 min, 8 min, and 2 min

for DMP) show up, and the peak intensity for the intermediates also changes as the reaction goes on. Based on mass analysis, the peak showing 209 (M-H)$^-$ at around 12 min retention time can be assigned to the mono-hydroxylated DMP (Figure S9), which is a typical primary intermediate in most •OH-dominated AOTs [15–17]. Since in the present study, the dominant reactive oxygen species should be •OH based on our previous study [23], hydroxylation is determined as one primary degradation pathway. Similar to DMP degradation, mono-hydroxylated DEP showing 237 (M-H)$^-$ at around 11.5 min was also found. In addition, monomethyl phthalate (MMP) showing 179 (M-H)$^-$ at around 8 min retention time was also detected, indicating another degradation pathway of DMP by oxidation of the aliphatic chain. Similarly, monoethyl phthalate (MEP) showing 193 (M-H)$^-$ was also identified as the primary intermediate for DEP degradation. Apart from the primary degradation intermediates, several secondary intermediates were also identified, like hydroxylated-MMP, hydroxylated-MEP, phthalate acid (PA), and hydroxylated-PA. Therefore, the possible degradation pathways of DMP and DEP are proposed in Figure 6. Although similar degradation pathways were identified for DMP and DEP, the TOC removal performance shows different degrees. No evident TOC removal was observed for both DMP and DEP during the ultrasonic degradation due to the fact that the •OH radicals mainly generate surrounding the cavitation bubbles not capable to react with more hydrophilic degradation intermediates. However, about 47% TOC was decreased for degrading 0.05 mM DMP and 35% was decreased for 0.05 mM DEP in US/Fe^{3+} + Vis/P25 process. This suggests that acceleration of Fe^{2+} regeneration can enhance the Fenton reaction and make the utilization of H$_2$O$_2$ more productive, so as to improve the mineralization of hydrophilic degradation intermediates.
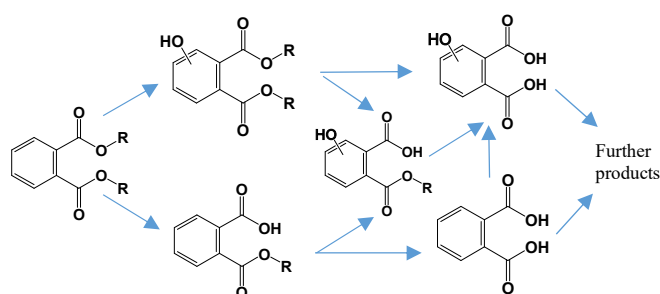

Figure 6. Possible degradation pathways of DMP and DEP.

3. Materials and Methods

3.1. Chemicals and Materials

Chemicals and materials used in this study are shown in Table S1 in Supplementary Materials. Ultrapure water prepared by water purification machine (Hhitech, Shanghai, China) was used exclusively. For pH adjustment, 0.1 M sulfuric acid (Sinopharm, Shanghai, China), and 0.1 M sodium hydroxide (Sinopharm, Shanghai, China) were used.

3.2. Apparatus and Experimental Conditions

The ultrasound apparatus used in this study is a stainless-steel basin-type reactor with 400 kHz frequency. The detailed description and set-up diagram are given elsewhere [17]. The experiments involving visible light were conducted using a commercial light emitting diode (LED) lamp and the emission spectrum is given in Figure S10, mainly covering the wavelength range from 400 to 600 nm. The radiation intensity was measured as 3575 μW·cm^{-2} at the surface position of the reaction solution via the 420 nm channel by Beijing Normal University Illuminometer. The solution volume of each test was kept constant as 250 mL unless otherwise indicated. The temperature of reaction solution was maintained at 25 ± 2 °C by cooling tube submerged in the solution which was made of the same material as that of the basin. No external stirring was applied for systems involving ultrasound and the suspension of P25 was realized by ultrasonic vibration. Quartz beaker was used

for the photocatalytic processes in which ultrasound was uninvolved. The initial concentration of target pollutants was 0.01 mM unless otherwise stated. The initial pH of reaction solution was kept constant at 3.5 ± 0.2, and neither further adjustment nor buffer was applied throughout. The dosage of P25 was kept constant at 0.5 g L^{-1} for experiments involving P25, except for the tests examining the effect of P25 dosages. As for the mixed liquids involving P25, it was allowed 15 min stirrer in beaker for adsorption equilibrium before being poured into the ultrasound reactor. Sample aliquots of exact 1.0 mL were withdrawn and quenched immediately with 0.2 mL methanol (TEDIA, Fairfield, OH, USA), and samples containing P25 were filtered by 0.2 μm membrane before analysis. All the experiments were duplicated or triplicated and the mean values were used for plotting.

3.3. Analytical Methods

The concentrations of DMP (Sigma-Aldrich, USA) and DEP (Sigma-Aldrich) were determined by high performance liquid chromatography (HPLC) (Dionex Ultimate 3000) equipped with a reverse-phase C18 column (5 μm particle size, 250 × 4.6 mm). The mobile phase for DMP and DEP measurement at a flow rate of 1.0 mL min^{-1} was composed of methanol and 0.1% phosphoric acid (Sigma-Aldrich, USA) water solution with a volume ratio of 60:40 and 70:30, respectively. The respective detection wavelength for DMP and DEP was 225 nm and 270 nm. The limit of detection (LOD) of the HPLC for DMP and DEP were determined as 0.0061 mg/L and 0.0048 mg/L, respectively (Text S1). The concentration of Fe^{2+} was determined by a spectrophotometric method by forming reddish orange complex with 1,10-phenanthroline (Sinopharm, Shanghai, China) ($\varepsilon = 1.1 \times 10^4$ L mol^{-1} cm^{-1}) which was detected at 510 nm. Intermediates identification was performed by HPLC/MS (LTQ Orbitrap XL, Thermo Fisher) equipped with an electrospray ionization source and an electrostatic orbitrap mass analyzer. The Agilent Polaris 3 C18-A column (5 μm particle size, 250 × 3.0 mm) was used for separation. Negative mode was used for intermediates detection. The mobile phase was obtained by mixing different ratio of methanol and water at the flow rate of 0.5 mL min^{-1} with the gradient program shown in Figure S2. The TOC concentration was quantified by Analytic Jena multi N/C 3100 TOC.

4. Conclusions

In this work, the synergistic effects and involved mechanisms of combining sono-Fenton and P25-based photocatalytic process under visible light have been investigated. Results show that, significant synergy (SI = 2.41 for Fe^{2+} precursor, SI = 2.68 for Fe^{3+} precursor) can be obtained at 0.02 mM iron dose, and more remarkable synergy is observed for more hydrophilic DMP compared with that for DEP. Generally, the influence of P25 on ultrasonic and sono-Fenton process in dark is weak. The direct photoreduction of Fe^{3+} only play a role at relatively high iron concentration (0.5 mM). The main mechanism of the synergy at low iron dose (0.02 mM) is found to be the fast regeneration of Fe^{2+} by photo-electrons provided by P25 photocatalysis. Both hydroxylation of aromatic ring and the oxidation of the aliphatic chain contribute to the degradation of DMP and DEP. Mineralization performance can also be enhanced by the combination of sono-Fenton and Vis/P25 process, and better mineralization performance is achieved for DMP (47%) than that for DEP (35%).

0.01 mM). Figure S8: Variation of ferrous ion concentrations during the degradation of DMP or DEP in visible light assisted sono-Fenton processes at two different levels of iron species: (a) 0.5 mM, (b) 0.02 mM ([DMP]$_0$ = 0.01 mM, [DEP]$_0$ = 0.01 mM). Figure S9: The profiles of HPLC spectra during the degradation of DMP and DEP ([DMP]$_0$ = 0.05 mM, [DEP]$_0$ = 0.05 mM, P25 dosage 0.5 g L^{-1}, [Fe^{3+}]$_0$ = 0.02 mM). Figure S10: The mass spectra of hydroxylated-dimethyl phthalate with m/z 210 and 209 (M-H)$^-$.

Author Contributions: Conceptualization, J.H. and L.X.; methodology, formal analysis, writing, L.Q. and W.L.; editing, G.T.; visualization, Y.S. All authors have read and agreed to the published version of the manuscript.

Conflicts of Interest: The authors declare no conflict of interest.

References

1. Bu, Q.; Wang, B.; Huang, J.; Deng, S.; Yu, G. Pharmaceuticals and personal care products in the aquatic environment in China: A review. *J. Hazard. Mater.* **2013**, *262*, 189–211. [CrossRef] [PubMed]

2. Glassmeyer, S.T.; Furlong, E.T.; Kolpin, D.W.; Batt, A.L.; Benson, R.; Boone, J.S.; Conerly, O.; Donohue, M.J.; King, D.N.; Kostich, M.S.; et al. Nationwide reconnaissance of contaminants of emerging concern in source and treated drinking waters of the United States. *Sci. Total Environ.* **2017**, *581*, 909–922. [CrossRef] [PubMed]

3. Ngoc Han, T.; Reinhard, M.; Gin, K.Y.-H. Occurrence and fate of emerging contaminants in municipal wastewater treatment plants from different geographical regions-a review. *Water Res.* **2018**, *133*, 182–207.

4. Cheng, M.; Zeng, G.; Huang, D.; Lai, C.; Xu, P.; Zhang, C.; Liu, Y. Hydroxyl radicals based advanced oxidation processes (AOPs) for remediation of soils contaminated with organic compounds: A review. *Chem. Eng. J.* **2016**, *284*, 582–598. [CrossRef]

5. Rao, Y.; Han, F.; Chen, Q.; Wang, D.; Xue, D.; Wang, H.; Pu, S. Efficient degradation of diclofenac by LaFeO$_3$-Catalyzed peroxymonosulfate oxidation-kinetics and toxicity assessment. *Chemosphere* **2019**, *218*, 299–307. [CrossRef] [PubMed]

6. Chen, M.; Huang, Y.; Chu, W. Exploring a broadened operating pH range for norfloxacin removal via simulated solar-light-mediated Bi$_2$WO$_6$ process. *Chin. J. Catal.* **2019**, *40*, 673–680. [CrossRef]

7. Gan, L.; Xu, L.; Qian, K. Preparation of core-shell structured CoFe$_2$O$_4$ incorporated Ag$_3$PO$_4$ nanocomposites for photocatalytic degradation of organic dyes. *Mater. Design.* **2016**, *109*, 354–360. [CrossRef]

8. Geng, A.; Meng, L.; Han, J.; Zhong, Q.; Li, M.; Han, S.; Mei, C.; Xu, L.; Tan, L.; Gan, L. Highly efficient visible-light photocatalyst based on cellulose derived carbon nanofiber/BiOBr composites. *Cellulose* **2018**, *25*, 4133–4144. [CrossRef]

9. Liu, C.; Liu, S.; Liu, L.; Tian, X.; Liu, L.; Xia, Y.; Liang, X.; Wang, Y.; Song, Z.; Zhang, Y.; et al. Novel carbon based Fe-Co oxides derived from Prussian blue analogues activating peroxymonosulfate: Refractory drugs degradation without metal leaching. *Chem. Eng. J.* **2020**, *379*, 379. [CrossRef]

10. Yang, L.; Xue, J.; He, L.; Wu, L.; Ma, Y.; Chen, H.; Li, H.; Peng, P.; Zhang, Z. Review on ultrasound assisted persulfate degradation of organic contaminants in wastewater: Influences, mechanisms and prospective. *Chem. Eng. J.* **2019**, *378*, 122146. [CrossRef]

11. Toscano, A.; Hellio, C.; Marzo, A.; Milani, M.; Lebret, K.; Cirelli, G.L.; Langergraber, G. Removal efficiency of a constructed wetland combined with ultrasound and UV devices for wastewater reuse in agriculture. *Environ. Technol.* **2013**, *34*, 2327–2336. [CrossRef] [PubMed]

12. Lobos-Moysa, E. Effect of pre-treatment and conditions on the appearance of long chain fatty acids in treatment of wastewater containing oil. *Desalin. Water. Treat.* **2018**, *134*, 148–153. [CrossRef]

13. Wong, L.-P.; Isa, M.H.; Bashir, M.J.K.; Yaqub, A. Low frequency ultrasound treatment of palm oil mill effluent for solubilization of organic matter. *Desalin. Water. Treat.* **2018**, *108*, 164–170. [CrossRef]

14. Torres-Palma, R.A.; Gibson, J.; Droppo, I.G.; Seto, P.; Farnood, R. Surfactant-assisted sono-breakage of wastewater particles for improved UV disinfection. *Water. Air. Soil. Poll.* **2017**, *228*, 106. [CrossRef]

15. Xu, L.J.; Chu, W.; Graham, N. Atrazine degradation using chemical-free process of USUV: Analysis of the micro-heterogeneous environments and the degradation mechanisms. *J. Hazard. Mater.* **2014**, *275*, 166–174. [CrossRef]

16. Xu, L.J.; Chu, W.; Graham, N. Sonophotolytic degradation of phthalate acid esters in water and wastewater: Influence of compound properties and degradation mechanisms. *J. Hazard. Mater.* **2015**, *288*, 43–50. [CrossRef]

17. Meng, L.; Gan, L.; Gong, H.; Su, J.; Wang, P.; Li, W.; Chu, W.; Xu, L. Efficient degradation of bisphenol A using high-frequency ultrasound: Analysis of influencing factors and mechanistic investigation. *J. Clean. Prod.* **2019**, *232*, 1195–1203. [CrossRef]

18. Zhou, X.; Yan, Y.; Li, Z.; Yin, J. Disinfection effect of a continuous-flow ultrasound/ultraviolet baffled reactor at a pilot scale. *Ultrason. Sonochem.* **2017**, *37*, 114–119. [CrossRef]

19. Xu, L.J.; Chu, W.; Graham, N. Sonophotolytic degradation of dimethyl phthalate without catalyst: Analysis of the synergistic effect and modeling. *Water Res.* **2013**, *47*, 1996–2004. [CrossRef]

20. Grcic, I.; Obradovic, M.; Vujevic, D.; Koprivanac, N. Sono-Fenton oxidation of formic acid/formate ions in an aqueous solution: From an experimental design to the mechanistic modeling. *Chem. Eng. J.* **2010**, *164*, 196–207. [CrossRef]

21. Ioan, I.; Wilson, S.; Lundanes, E.; Neculai, A. Comparison of Fenton and sono-Fenton bisphenol A degradation. *J. Hazard. Mater.* **2007**, *142*, 559–563. [CrossRef] [PubMed]

22. Shen, Y.; Xu, Q.; Wei, R.; Ma, J.; Wang, Y. Mechanism and dynamic study of reactive red X-3B dye degradation by ultrasonic-assisted ozone oxidation process. *Ultrason. Sonochem.* **2017**, *38*, 681–692. [CrossRef] [PubMed]

23. Xu, L.; Zhang, X.; Han, J.; Gong, H.; Meng, L.; Mei, X.; Sun, Y.; Qi, L.; Gan, L. Degradation of emerging contaminants by sono-Fenton process with in situ generated H_2O_2 and the improvement by P25-mediated visible light irradiation. *J. Hazard. Mater.* **2020**, *391*, 122229. [CrossRef] [PubMed]

24. Xu, T.; Zhu, R.; Zhu, G.; Zhu, J.; Liang, X.; Zhu, Y.; He, H. Mechanisms for the enhanced photo-Fenton activity of ferrihydrite modified with $BiVO_4$ at neutral pH. *Appl. Catal. B Environ.* **2017**, *212*, 50–58. [CrossRef]

25. Zhu, Y.; Zhu, R.; Yan, L.; Fu, H.; Xi, Y.; Zhou, H.; Zhu, G.; Zhu, J.; He, H. Visible-light Ag/AgBr/ferrihydrite catalyst with enhanced heterogeneous photo-Fenton reactivity via electron transfer from Ag/AgBr to ferrihydrite. *Appl. Catal. B Environ.* **2018**, *239*, 280–289. [CrossRef]

26. Xu, L.; Meng, L.; Zhang, X.; Mei, X.; Guo, X.; Li, W.; Wang, P.; Gan, L. Promoting Fe^{3+}/Fe^{2+} cycling under visible light by synergistic interactions between P25 and small amount of Fenton reagents. *J. Hazard. Mater.* **2019**, *379*, 120795. [CrossRef]

27. Bui, T.T.; Giovanoulis, G.; Cousins, A.P.; Magner, J.; Cousins, I.T.; de Wit, C.A. Human exposure, hazard and risk of alternative plasticizers to phthalate esters. *Sci. Total Environ.* **2016**, *541*, 451–467. [CrossRef]

28. Rodriguez, E.M.; Marquez, G.; Tena, M.; Alvarez, P.M.; Beltran, F.J. Determination of main species involved in the first steps of TiO_2 photocatalytic degradation of organics with the use of scavengers: The case of ofloxacin. *Appl. Catal. B Environ.* **2015**, *178*, 44–53. [CrossRef]

29. Pan, X.; Yang, M.-Q.; Fu, X.; Zhang, N.; Xu, Y.-J. Defective TiO_2 with oxygen vacancies: Synthesis, properties and photocatalytic applications. *Nanoscale* **2013**, *5*, 3601–3614. [CrossRef]

30. Liu, Y.; Wu, D.; Peng, S.; Feng, Y.; Liu, Z. Enhanced mineralization of dimethyl phthalate by heterogeneous ozonation over nanostructured Cu-Fe-O surfaces: Synergistic effect and radical chain reactions. *Sep. Purif. Technol.* **2019**, *209*, 588–597. [CrossRef]

31. Xu, L.; Qi, L.; Sun, Y.; Gong, H.; Chen, Y.; Pei, C.; Gan, L. Mechanistic studies on peroxymonosulfate activation by g-C_3N_4 under visible light for enhanced oxidation of light-inert dimethyl phthalate. *Chin. J. Catal.* **2020**, *41*, 322–332. [CrossRef]

32. Adewuyi, Y.G. Sonochemistry: Environmental science and engineering applications. *Ind. Eng. Chem. Res.* **2001**, *40*, 4681–4715. [CrossRef]

33. Neyens, E.; Baeyens, J. A review of classic Fenton's peroxidation as an advanced oxidation technique. *J. Hazard. Mater.* **2003**, *98*, 33–50. [CrossRef]

34. Pang, Y.L.; Abdullah, A.Z.; Bhatia, S. Review on sonochemical methods in the presence of catalysts and chemical additives for treatment of organic pollutants in wastewater. *Desalination* **2011**, *277*, 1–14. [CrossRef]

35. Adityosulindro, S.; Barthe, L.; Gonzalez-Labrada, K.; Jauregui Haza, U.J.; Delmas, H.; Julcour, C. Sonolysis and sono-Fenton oxidation for removal of ibuprofen in (waste) water. *Ultrason. Sonochem.* **2017**, *37*, 889–896. [CrossRef] [PubMed]

36. National Library of Medicine. Available online: https://pubchem.ncbi.nlm.nih.gov/ (accessed on 5 October 2020).

37. Braterman, P.S.; Cairns-Smith, A.G.; Sloper, R.W.; Truscott, T.G.; Craw, M. Photo-oxidation of iron(II) in water between pH 7.5 and 4.0. *J. Chem. Soc. Dalton Trans.* **1984**, 1441–1445. [CrossRef]

38. Airey, P.L.; Dainton, F.S. The photochemistry of aqueous solutions of Fe (II). I. Photoelectron detachment from ferrous and ferrocyanide ions. *Proc. R. Soc. London Ser. A Math. Phys. Sci.* **1966**, *291*, 340–352.